

Comparison of computational model and X-ray crystal structure of human serotonin transporter: potential application for the pharmacology of human monoamine transporters

Fengyuan Yang, Tingting Fu, Xiaoyu Zhang, Jie Hu, Weiwei Xue, Guoxun Zheng, Bo Li, Yinghong Li, Xiaojun Yao & Feng Zhu

To cite this article: Fengyuan Yang, Tingting Fu, Xiaoyu Zhang, Jie Hu, Weiwei Xue, Guoxun Zheng, Bo Li, Yinghong Li, Xiaojun Yao & Feng Zhu (2017): Comparison of computational model and X-ray crystal structure of human serotonin transporter: potential application for the pharmacology of human monoamine transporters, Molecular Simulation, DOI: [10.1080/08927022.2017.1309653](https://doi.org/10.1080/08927022.2017.1309653)

To link to this article: <http://dx.doi.org/10.1080/08927022.2017.1309653>



Published online: 16 May 2017.



Submit your article to this journal



Article views: 29



View related articles



View Crossmark data

Full Terms & Conditions of access and use can be found at
<http://www.tandfonline.com/action/journalInformation?journalCode=gmos20>



Comparison of computational model and X-ray crystal structure of human serotonin transporter: potential application for the pharmacology of human monoamine transporters

Fengyuan Yang^a, Tingting Fu^a, Xiaoyu Zhang^a, Jie Hu^a, Weiwei Xue^a, Guoxun Zheng^a, Bo Li^a, Yinghong Li^a, Xiaojun Yao^b and Feng Zhu^a

^aInnovative Drug Research and Bioinformatics Group, School of Pharmaceutical Sciences and School of Public Affairs, Chongqing University, Chongqing, P.R. China; ^bState Key Laboratory of Applied Organic Chemistry and Department of Chemistry, Lanzhou University, Lanzhou, P.R. China

ABSTRACT

The human serotonin transporter (hSERT) played a significant role in neurological process whose structural basis had been analysed for many years. Recently, the first homology model was constructed for hSERT based on the crystal structure of *drosophila melanogaster* dopamine transporter was published, and the inhibitory mechanism underlying the binding mode between hSERT and approved antidepressants was substantially investigated by molecular dynamics (MD) simulation. Right after this publication, the X-ray crystallographic structures of hSERT were reported, which provided a good opportunity to reassess the performance of previous simulation. In this study, the analyses of side-chain contact map, stereochemical quality and ligand-binding pocket were firstly conducted, which revealed that the constructed homology model of hSERT could successfully reproduce the reported crystal structure. Secondly, the approved antidepressant escitalopram was docked into the X-ray structure, and its binding pose was consistent with the reported docking pose in the homology model. Finally, MD simulation were performed based on the crystal structure of hSERT, and structural features revealed as critical for escitalopram-hSERT interaction by previous simulation were successfully recaptured. Thus, the newly reported X-ray crystal structure of hSERT was precisely predicted by computational model, which demonstrated its reliability in understanding the pharmacology of other human monoamine transporters whose 3-D structure remained unknown.

ARTICLE HISTORY

Received 21 January 2017
Accepted 16 March 2017

KEYWORDS

Human serotonin transporter; escitalopram; homology modelling; docking; molecular dynamics

1. Introduction

Antidepressants were widely used for the treatment of patients with major depression disorder and other mood disorder diseases [1–4]. Whereby, the selective serotonin reuptake inhibitors (SSRIs) were most commonly used to inhibit the function of human serotonin transporter (hSERT) [2,4,5], which indirectly block the serotonin signal transmission in the synaptic cleft [6–8]. As the major target for SSRIs, hSERT played critical roles in the process of terminating serotonergic signalling through the reuptake of serotonin into presynaptic neurons [9]. During the period of new antidepressant drugs design, the exact molecular interaction pattern of SSRIs and hSERT was proved crucial to reveal drug inhibitory mechanism and further new antidepressant inhibitors design [10–14]. So, on the basis of the structures of the *drosophila melanogaster* dopamine transporter (dDAT) [15], a hSERT homology model was generated. Additionally, the structural features of FDA approved SSRIs binding with hSERT were further analysed by molecular docking and MD simulation [16]. The detailed interaction pattern shared by the approved drugs was identified which consists of 11 hotspots residues in hSERT and three chemical groups of the FDA approved SSRIs.

Right after this publication, hSERT's crystal structure was solved [9]. This structure provided a good chance to reassess the results of the constructed computational model in the previous work.

In this study, the reliability of the constructed homology model of hSERT was systematically reassessed in comparison with X-ray crystallographic structure. Firstly, side-chain contact map and stereochemical quality of both structures were carried out to analyse the quality of the homology model. Then, the root-mean-square deviation values (RMSD) of the 11 amino acids that compose the ligand binding pocket (LBP) was calculated, and the value (0.6 Å) demonstrating a reliable hSERT model. Finally, a long-lasting MD simulation was carried and revealed consistent key residues for drug binding in both homology model and crystal complexes.

2. Materials and methods

2.1. Homology modelling of hSERT

Based on the high sequence identity of hSERT with dDAT (53%), as shown in Figure 1, dDAT crystal structure (PDB code 4M48 [15]) was chosen as the template for the homology model

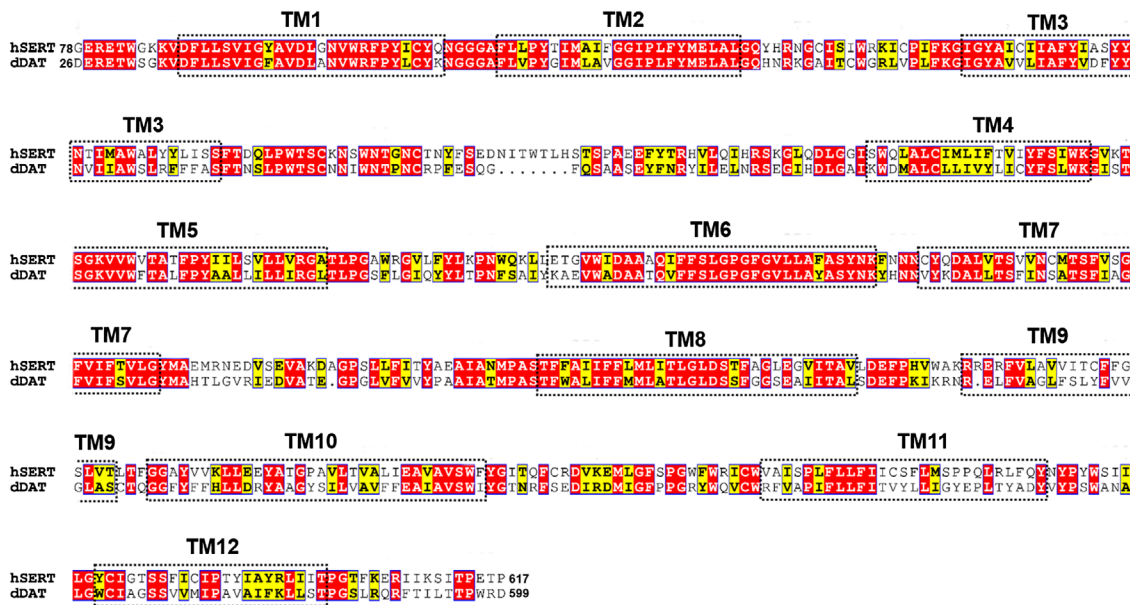


Figure 1. (Colour online) Sequence alignment of hSERT (from Glu78 to Pro617) and dDAT (from Glu26 to Asp599) using ClustalX program. The twelve transmembrane (TM1 to TM12) alpha helices are labelled with the black dotted box. The red shadow periods refer to the identical residues, the yellow shadow periods refer to the conservative substitutions.

construction. And SWISS-MODEL in an automated mode were used [17]. The constructed model comprised amino acids 78–617 that concluded the crucial 12 transmembrane regions as well as the corresponding intervening loops. To validate the constructed homology model, Ramachandran plot in PROCHECK [18] was further applied. In addition, two functional Na^+ in LeuBAT [19] were introduced into the corresponding locations of binding site by superimposing the model and LeuBAT structure together via PyMOL's [20].

2.2. Model evaluation

2.2.1. Side chain contact map analysis

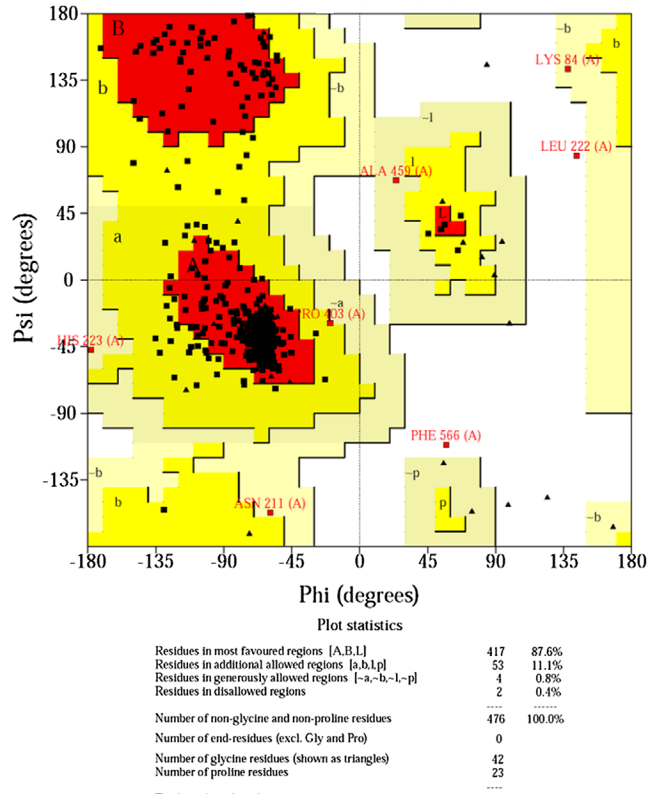
Here, the analysis was taken for both the homology model and X-ray structure of hSERT by program SPACE [21]. For contact map analysis, residue–residue contacts with the studied proteins are depicted as an interactive contact map, and the square at the crossing of two residues rightly indicates the contacts.

2.2.2. Stereochemical quality analysis

Stereochemistry qualities of each overall model were evaluated using ProSA [22]. The knowledge-based potentials [23] were used in the calculation process of assessing model accuracy, as a result, a Z-score value for each input structure was generated. The Z-score measures the deviation between the total energy of the structure and the energy distribution derived from random conformations [23].

2.2.3. RMSD analysis

RMSD is the most common check to measure structural similarity between a model and a correct structure. The RMSD values between molecules were calculated using VMD Plugin RMSD Tool [24] based on the selected groups of atoms after an optimal superposition.



Based on an analysis of 118 structures of resolution of at least 2.0 Angstroms and R-factor no greater than 20%, a good quality model would be expected to have over 90% in the most favoured regions.

Figure 2. (Colour online) Ramachandran plot of the hSERT model.

2.3. Molecular docking

2.3.1. Docking of escitalopram to hSERT homology model

Site-directed mutagenesis study showed that Tyr95, Asp98,

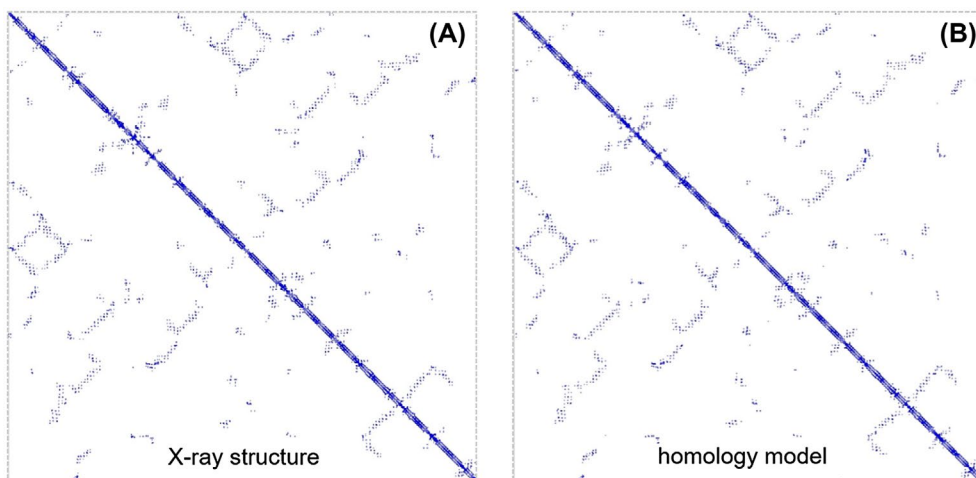


Figure 3. (Colour online) Side chains contact plot for X-ray structure (A) and homology model (B) of hSERT.

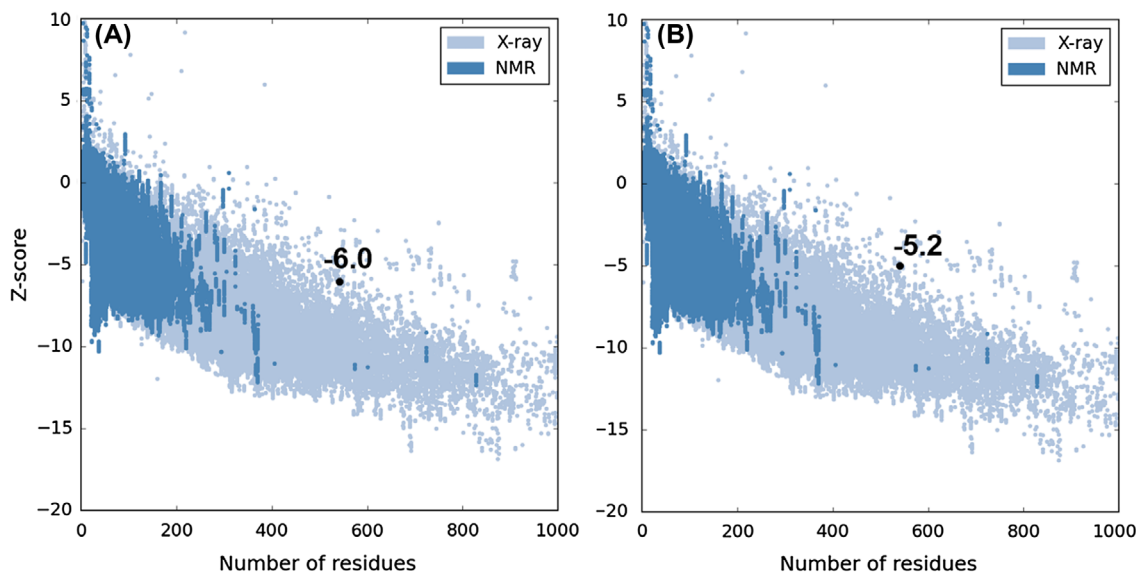


Figure 4. (Colour online) Z-score plot for homology model (A) and X-ray structure of hSERT (B).

Ile172, Asn177, Phe341 and Ser438 of hSERT are critical for escitalopram binding [25]. Therefore, the initial binding pose of escitalopram to hSERT was obtained by docking the drug into a grid box defined by the six residues in the modelled structure of hSERT. The docking procedure was performed by Glide software [12] with the default settings of standard precision mode.

2.3.2. Re-docking of escitalopram to hSERT crystal structure

To test the reproducibility of docking tool, the X-ray structures of hSERT complexed with escitalopram (PDB code 5I71 [9]) was used for re-docking by Glide software [12]. Then, the LigPrep [13] with OPLS-2005 force field [26] was used to pre-process the structure of escitalopram and resulted in a low-energy conformation. The ionised state was assigned by Epik [17] under the circumstance of a pH value of 7.0 ± 2.0 . Hydrogen atoms were added using the Protein Preparation Wizard module in Maestro [19], meanwhile, partial charges as well as the protonation states were assigned by OPLS-2005 force field [26]. Thus,

a prepared hSERT structure was ready for docking. Before docking, a minimization process was carried and terminated till the root-mean-square-deviation reached to the maximum value (0.30 \AA). Then, escitalopram was docked into the protein with the grid box defined by centring on drug in protein via the Receptor Grid Generation tool in Glide [26]. In the initial phase of docking, 5000 poses in all were generated and the most rational 400 poses were selected for the following 100 steps of conjugate gradient minimization.

2.4. MD simulation

2.4.1. System preparation

The initial structure for escitalopram binding with hSERT was obtained from the RCSB Bank (PDB code 5I71 [9]). Firstly, the calculation of spatial orientations of the complexes was performed by OPM [27], and was inserted into a POPC lipid bilayer with water thickness of 20 \AA and 0.15 M of NaCl using

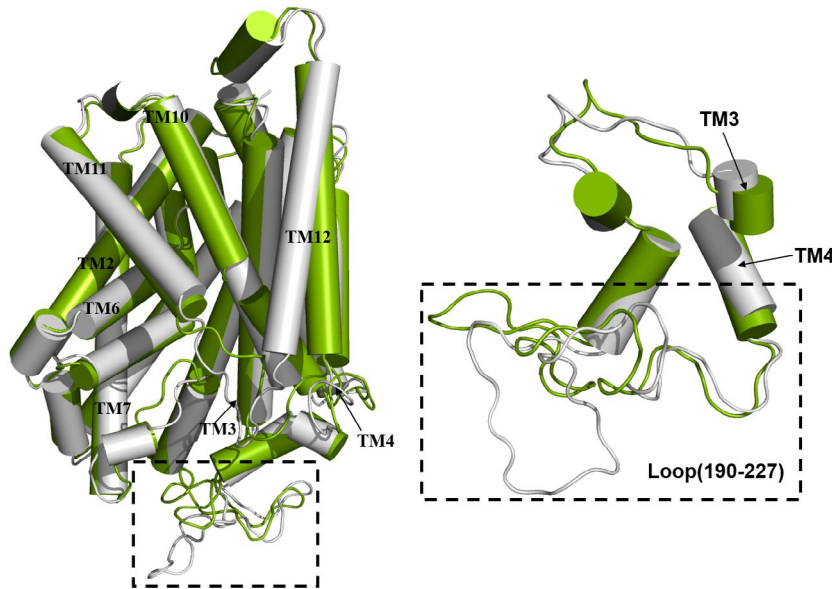


Figure 5. (Colour online) Superimposition of hSERT X-ray structure (PDB code 5I71 [6]) and the homology model. Helices are depicted as cylinders, β -sheets as arrows, random-coil as tube. X-ray structure and homology model are coloured in grey and green, respectively.

Table 1. Root-mean-square-deviation (RMSD, in Å) after superimposition of the homology model and X-ray structure (PDB code 5I71 [6]).

All residues	Disregard the flexible extracellular loops	Ligand binding pocket
2.5	1.7	0.6

CHARMM-GUI Membrane Builder [28]. Then, AMBER force field ff14SB [29] and Lipid14 [30] were chosen for proteins and lipids, respectively. The General AMBER Force Field was applied to define the force field parameters and the restrained electrostatic potential partial charges in antechamber were applied to assign charges. Gaussian09 was taken for the calculation of the Geometry optimisation and electrostatic potential under condition of HF/6-31G* level [25]. The size of each system was ~96,000 atoms, with the periodic box was set as 83 Å × 83 Å × 127 Å.

2.4.2. Performing the molecular dynamics simulation

The AMBER14 [31] software along with GPU-accelerated PMEMD was taken for the MD simulation. Then, the following minimization, heating and equilibration process were carried on each simulation. A 150 ns simulation under a periodic boundary condition was performed in an NPT ensemble with temperature and pressure settled as 310 K and 1 atm, respectively. In the meantime, particle-mesh Ewald method was applied for the calculation of the direct space in consideration of the long-range electrostatic interaction (cutoff = 10.0 Å) [32]. Constraints by the SHAKE algorithm [33] were exerted to all bonds of the system while the integration time was settled as 2 fs.

2.5. Binding free energy calculation

With no consideration of the entropic contribution, the $\Delta G_{\text{MM/GBSA}}$ of escitalopram binding with hSERT was calculated by the MM/GBSA method [34–38]. Here, 500 snapshots extracted from the last 50 ns simulation trajectory were chosen

for energy calculation. The $\Delta G_{\text{MM/GBSA}}$ was calculated for each snapshot as below:

$$\Delta G_{\text{MM/GBSA}} = \Delta E_{\text{vdW}} + \Delta E_{\text{ele}} + \Delta G_{\text{pol}} + \Delta G_{\text{nonpol}} \quad (1)$$

The van der Waals and electrostatic contribution calculated under the gas phase condition are depicted as ΔE_{vdW} and ΔE_{ele} , and ΔE_{pol} and ΔE_{nonpol} are regarded as the polar and the non-polar solvent interaction energies, respectively. ΔG_{nonpol} was calculated according to the equation $\Delta G_{\text{nonpol}} = 0.0072 - \Delta \text{SASA}$ by the linear combination of the pairwise overlap method [39], and the SASA refers to the solvent accessible area.

2.6. Per-residue energy decomposition analysis

To explore the detailed contribution of each residue, the binding energy calculated above was decomposed into each residue. The binding free energy ($\Delta G_{\text{MM/GBSA}}^{\text{per residue}}$) without considering the entropic contribution was calculated according to:

$$\Delta G_{\text{MM/GBSA}}^{\text{per residue}} = \Delta E_{\text{vdW}}^{\text{per residue}} + \Delta E_{\text{ele}}^{\text{per residue}} + \Delta G_{\text{pol}}^{\text{per residue}} + \Delta G_{\text{nonpol}}^{\text{per residue}} \quad (2)$$

The definition of van der Waals ($\Delta E_{\text{vdW}}^{\text{per residue}}$), electrostatic contribution ($\Delta E_{\text{ele}}^{\text{per residue}}$) and the polar ($\Delta G_{\text{pol}}^{\text{per residue}}$) is in accordance with that in Equation (1), except for the non-polar solvent interaction energy ($\Delta G_{\text{nonpol}}^{\text{per residue}}$). The $\Delta G_{\text{nonpol}}^{\text{per residue}}$ is defined as the periodic approximation of sphere around atoms of an icosahedron (ICOSA) [31].

3. Results and discussion

3.1. Quality of the hSERT homology model

The structure of the modelled hSERT covered all 12 transmembrane α -helices. There were no significant differences in these helices of the homology model observed when compared to

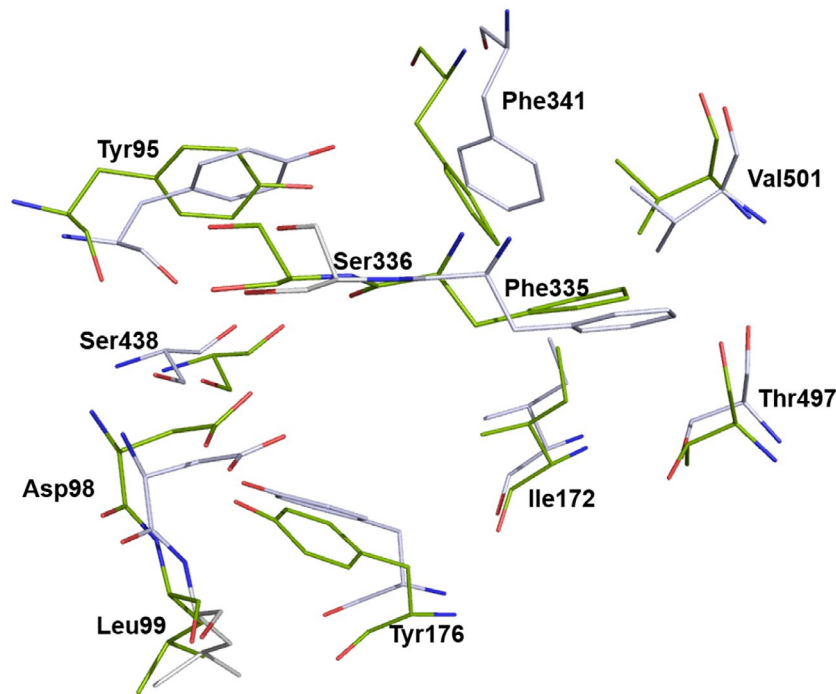


Figure 6. (Colour online) Accuracy of ligand binding pocket (LBP) modelling. Side-chain conformations of 11 amino acids lining the LBP. Residues of the X-ray structure (PDB code 5I71 [6]) are coloured in purple whereas amino acids of the homology model are shown in green.

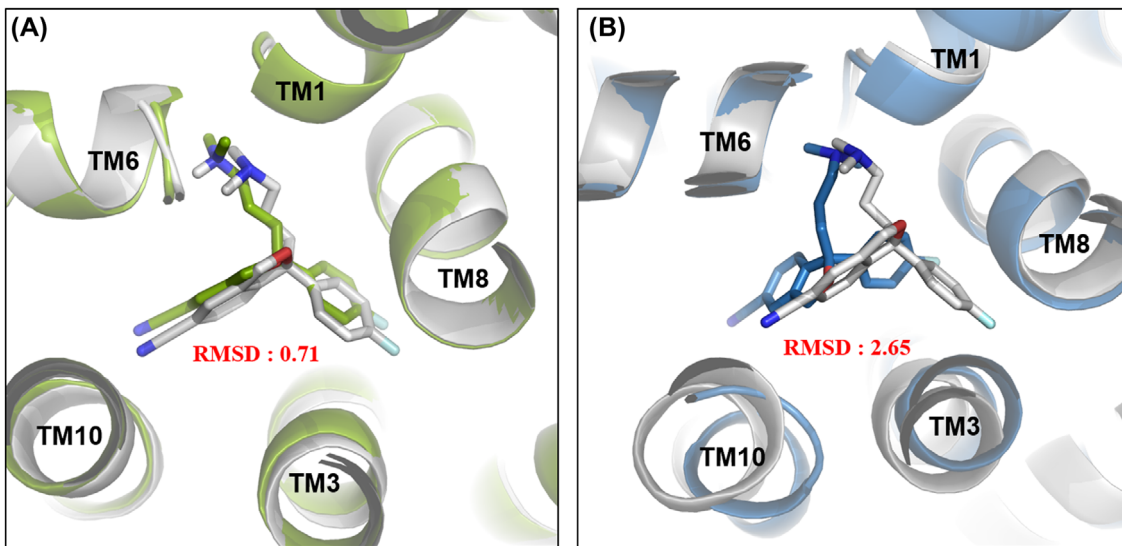


Figure 7. (Colour online) Pose of escitalopram docked into the X-ray structure (A) and homology model (B) in comparison with that observed in the X-ray structure. Carbon atoms of the co-crystallised ligand are depicted as grey stick. Docking poses are shown in green and blue stick for X-ray structure and homology model, respectively.

the reported X-ray crystal results [40]. Ramachandran plot in PROCHECK showed 99.5% residues in allowed regions as shown in Figure 2, indicating a reliable homology model.

To further evaluate how well the homology model fit to the X-ray crystal structure of hSERT, a comparison of these two structures was made through geometrical and statistical analysis. Side-chain contact map displayed a very similar profile between these structures (Figure 3). Simultaneously, Z-score analysis (Figure 4) was taken for evaluating the quality of the homology model from a stereochemical aspect, and the Z-score

value of the homology model (-6.0) is close to that of the crystal structure (-5.2).

Figure 5 illustrated the structural superimposition results of the homology model and crystal structure, the overall distribution of all helices and loops matched pretty well except for the region connecting TM3 and TM4 (residues 190–227). The RMSD value of the backbone atoms between homology model and crystal structure was 2.5 Å, suggesting an optimal modelling quality (Table 1). Moreover, disregarding the flexible extracellular loops, the RMSD value fell to 1.7 Å.

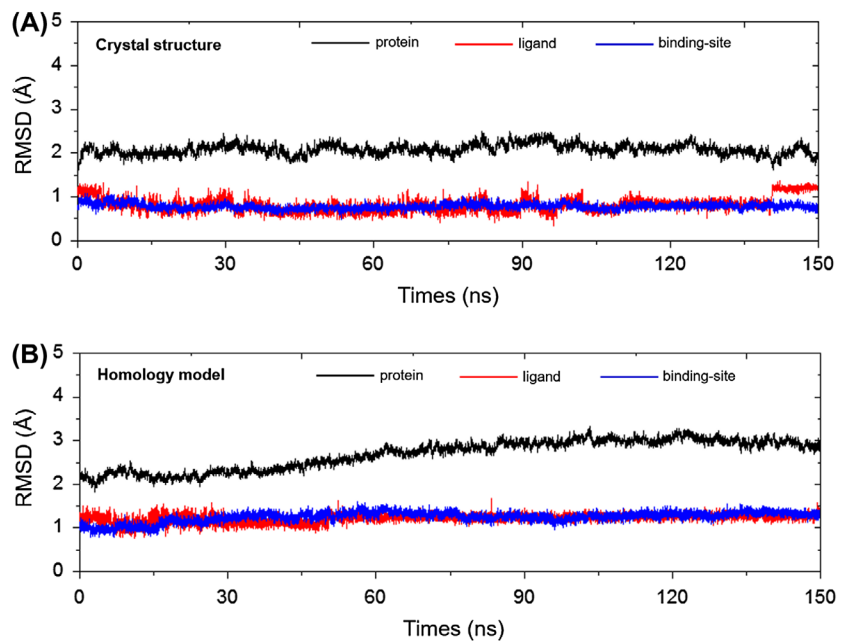


Figure 8. (Colour online) RMSD of protein backbone atoms (black), ligand heavy atoms (red) and binding site residue backbone atoms (blue) of the escitalopram-bound hSERT crystal structure (A) and homology model (B) against the simulation time.

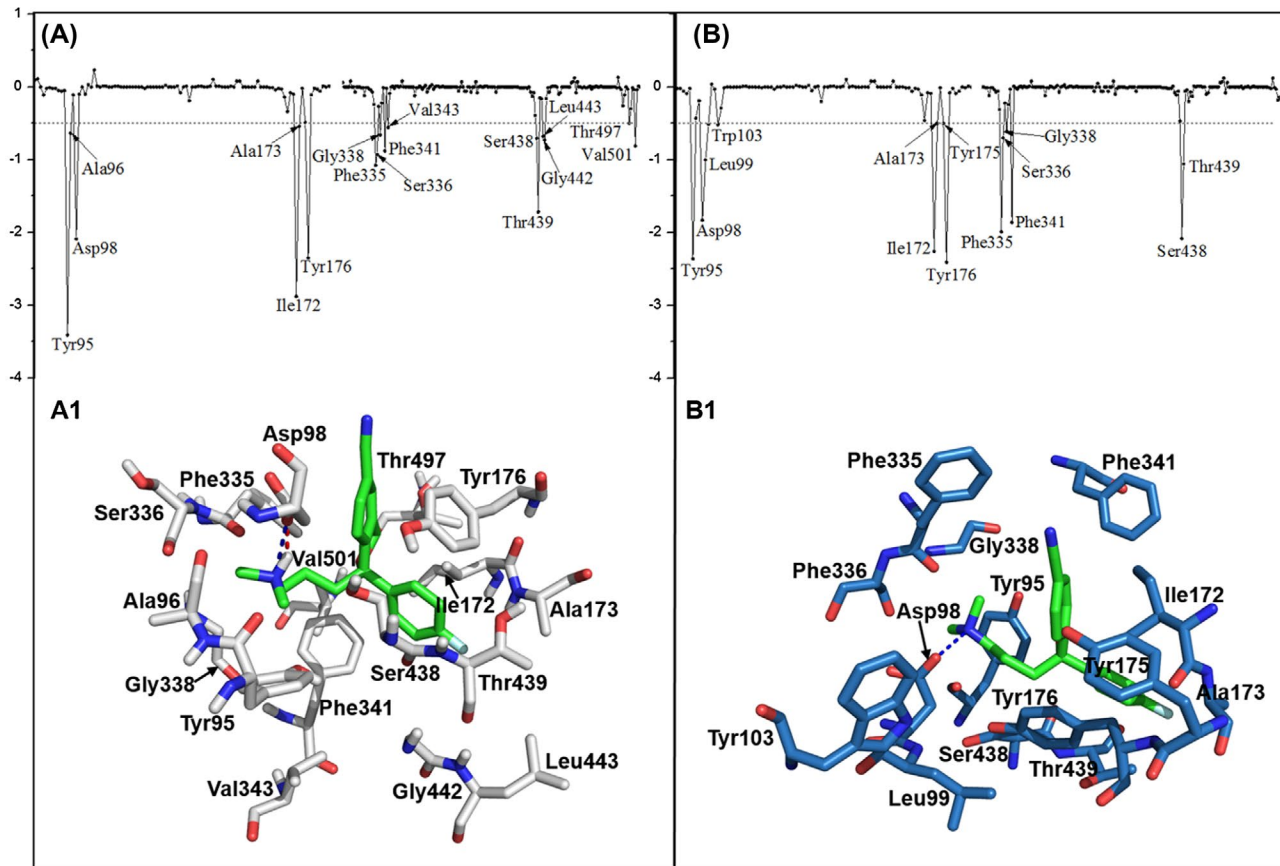


Figure 9. (Colour online) Energetic contributions of each individual amino acid residue of X-ray (A) and homology model (B) of hSERT binding with escitalopram. Below are the corresponding average structures from the MD simulation with the identified key residues of the binding pocket. The side chains of the residues are shown as a stick drawing (in grey and blue for X-ray and homology model, respectively) and escitalopram is represented as a stick drawing (in green).

Table 2. The calculated binding free energies of studied inhibitor escitalopram binding to homology model and crystal structure of hSERT (ΔG is in kcal/mol).

	ΔE_{ele}	ΔE_{vdW}	ΔG_{pol}	ΔG_{nonpol}	$\Delta G_{MM/GBSA}$
Model	-31.98 ± 0.20	-47.66 ± 0.11	36.67 ± 0.17	-6.24 ± 0.01	-49.21 ± 0.12
Crystal	-32.60 ± 0.24	-47.66 ± 0.11	36.90 ± 0.17	-6.04 ± 0.01	-49.40 ± 0.11

For further assessing the accuracy of the homology model, a structure superimposition was made for the amino acids composing the ligand binding pocket (LBP) (Figure 6). Moreover, the RMSD value was calculated for the backbone atoms of the 11 amino acids located at the binding site and the result was 0.6 Å. The results further demonstrated the high reliability of the homology model constructed methods used in previous work. The mis-prediction in the region (residues 190–227) made negligible effect on the reliability of fundamental regions of hSERT model, since the flexible loop region (residues 190–227) is distributed at the protein surface. In particular, the residues located there do not participate in the formation of ligand-binding pocket.

3.2. Reproduction of escitalopram-binding modes in co-crystal structure

In our previous work, the initial structural model of escitalopram in complex with hSERT were obtained by re-docking using Glide software [26]. To reassess the accuracy of the docking results in previous work, escitalopram was first docked into the X-ray crystal structure. The binding pose of escitalopram obtained by docking is close to the conformation in crystal structure with the RMSD value of 0.71 Å (Figure 7(A)). In addition, the binding pose of escitalopram in complex with homology model is quite similar with that in the co-crystal structure with the RMSD value of 2.65 Å (Figure 7(B)).

3.3. Comparison of the identified key residues contributing to drug binding

After getting the initial structural model of escitalopram-hSERT complex, MD simulation followed by binding energy calculation was applied to identify the key residues contributing to drug binding [16]. To explore the key residues involved in the drug binding in crystal structures, a 150 ns MD simulation in explicit solvent was carried on the X-ray crystallographic structure of hSERT bound with escitalopram. The RMSD analysis of protein backbone atoms, ligand heavy atoms and binding site residue backbone atoms of the escitalopram-bound hSERT crystal (Figure 8(A)) against the simulation time was applied to monitor the simulation stability. As a comparison, the RMSD analysis for the escitalopram-bound homology model in our previous work was also shown (Figure 8(B)). By means of binding free energy calculation for the simulation, we proposed that the inhibition of hSERT is mainly consisted of electrostatic interaction and van der Waals interaction (Table 2). Table 2 showed that the calculated binding energy of the escitalopram-bound homology model is in good consistence with that of crystal structure.

Then, a thorough evaluation illustrating the contribution of each amino acid was made to reassess the binding mode in detail. MM/PBSA energy decomposition analysis was applied for the calculation of each amino acid and the results were shown in Figure 9. As shown in Figure 9(A) and (B), 11 residues (with enthalpy contribution ≥ 0.5 kcal/mol) including Tyr95, Asp98, Ile172, Ala173, Tyr176, Phe335, Phe341, Ser336, Gly338, Ser438 and Thr439 were identified as key amino acids contributing to escitalopram binding with homology model and crystal structure. Figure 9 also illustrated the representative snapshot of

escitalopram-hSERT complex from equilibrated MD trajectories, illustrating the binding pose of escitalopram in hSERT and key interacting residues. As shown in Figure 9(A1) and (B1), escitalopram shares a similar orientation in the hSERT homology model and crystal structure. The protonation N moiety of escitalopram mainly engaged in the formation of salt bridge interaction and hydrogen bond with Asp98. The benzene substitutions are extended to hydrophobic cavity formed by residues Tyr95, Ile172, Ala173, Tyr176 and Phe335, Phe341, Ser336, Gly338 and also with Ser438 and Thr439, respectively. The comparison of the detailed interaction pattern between the hSERT homology model and crystal structure further verified our homology model.

In addition, the decomposition energy contribution of the residues in the loop region (residue 190–227) was shown in Table 3. Residues in this region barely made contribution to the binding of escitalopram with hSERT except the residues Asp193, Lys201, Cys209, Glu215 and Asp216. And, only residues Asp193, Glu215 and Asp216 were reflected by the conformation change in this region, but these impacts could be neglected compared to the total energy contribution. Even the conformation changes of this region shown in Figure 5 are quiet evident, the conformation changes had negligible impact on the binding of escitalopram with hSERT. The results further verified the reliability of our model structure.

Table 3. The calculated binding free energies of residues in the TM3 and TM4 loop region (residue 190–227) of studied inhibitor escitalopram binding to homology model and crystal structure of hSERT (ΔG is in kcal/mol).

	Homology model				Crystal structure			
	ΔG	ΔE_{vdw}	ΔE_{ele}	ΔE_{pol}	ΔG	ΔE_{vdw}	ΔE_{ele}	ΔE_{pol}
Ser190	0	0	0.05	-0.05	0	0	0.05	-0.05
Pho191	0	0	0.04	-0.04	0	0	0.04	-0.04
Thr192	0	0	-0.03	0.03	0	0	-0.03	0.03
Asp193	-0.05	0	-2.18	2.13	-0.05	0	-2.18	2.13
Gln194	0	0	0.02	-0.02	0	0	0.02	-0.02
Leu195	0	0	0.06	-0.06	0	0	0.06	-0.06
Pro196	0	0	0.05	-0.05	0	0	0.05	-0.05
Trp197	0	0	0.03	-0.03	0	0	0.03	-0.03
Thr198	0	0	0.04	-0.04	0	0	0.04	-0.04
Ser199	0	0	0.02	-0.02	0	0	0.02	-0.02
Cys200	0	0	0.01	-0.01	0	0	0.01	-0.01
Lys201	0.05	0	2.08	-2.03	0.05	0	2.08	-2.03
Asn202	0	0	0.04	-0.04	0	0	0.04	-0.04
Ser203	0	0	0.01	-0.01	0	0	0.01	-0.01
Trp204	0	0	0.02	-0.02	0	0	0.02	-0.02
Asn205	0	0	0.01	-0.01	0	0	0.01	-0.01
Thr206	0	0	0.02	-0.02	0	0	0.02	-0.02
Gly207	0	0	0	0	0	0	0	0
Asn208	0	0	0	0	0	0	0	0
Cys209	0	0	0.03	-0.03	0	0	0.03	-0.03
Thr210	0	0	-0.01	0.01	0	0	-0.01	0.01
Asn211	0	0	0.02	-0.02	0	0	0.02	-0.02
Tyr212	0	0	0.02	-0.02	0	0	0.02	-0.02
Phe213	0	0	-0.01	0.01	0	0	-0.01	0.01
Ser214	0	0	0.02	-0.02	0	0	0.02	-0.02
Glu215	-0.07	0	-2.75	2.68	-0.07	0	-2.75	2.68
Asp216	-0.06	0	-2.22	2.17	-0.06	0	-2.22	2.17
Asn217	0	0	-0.01	0.01	0	0	-0.01	0.01
Ile218	0	0	-0.05	0.05	0	0	-0.05	0.05
Thr219	0	0	0.05	-0.04	0	0	0.05	-0.04
Trp220	0	0	0.02	-0.02	0	0	0.02	-0.02
Thr221	0	0	0.02	-0.02	0	0	0.02	-0.02
Leu222	0	0	-0.02	0.02	0	0	-0.02	0.02
Hie223	0	0	0.02	-0.02	0	0	0.02	-0.02
Ser224	0	0	-0.03	0.03	0	0	-0.03	0.03
Thr225	0	0	0.07	-0.07	0	0	0.07	-0.07
Ser226	0	0	-0.02	0.02	0	0	-0.02	0.02
Pro227	0	0	-0.03	0.02	0	0	-0.03	0.02

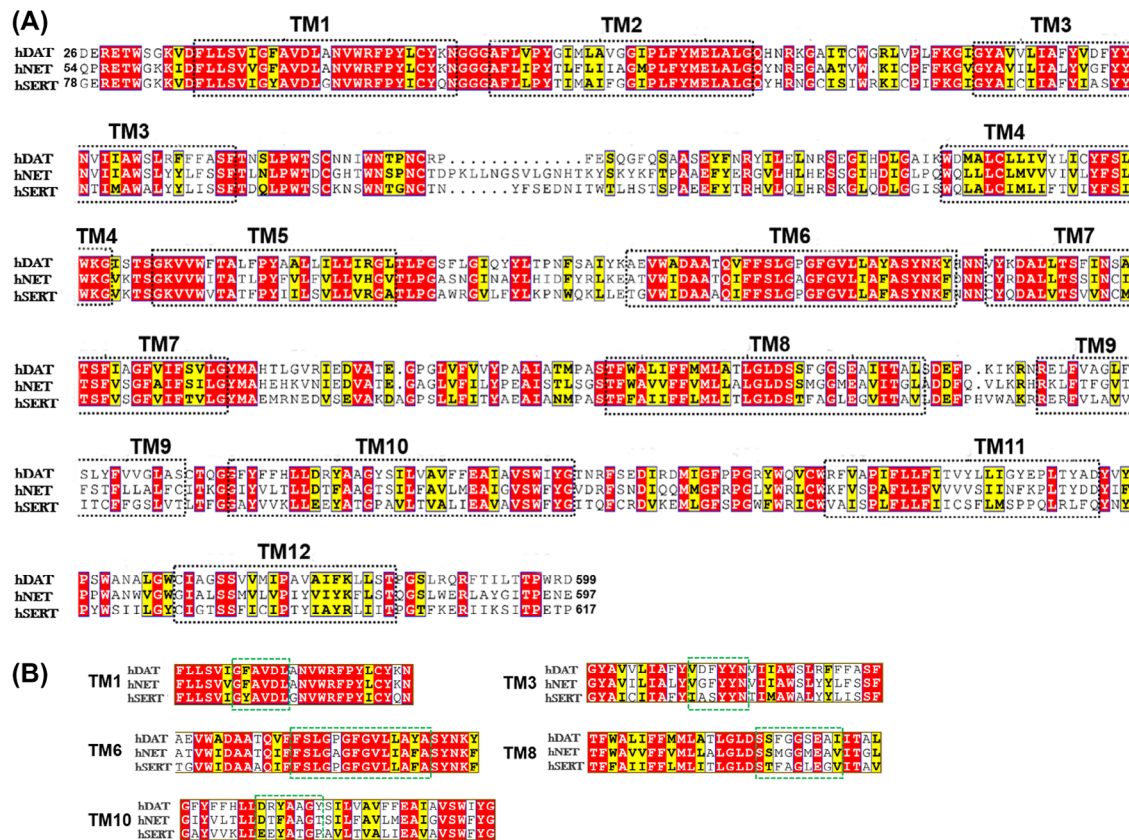


Figure 10. (Colour online) (A) Sequence alignment of hSERT (from Glu78 to Pro617), hNET (from Gln54 to Glu597) and dDAT (from Glu26 to Asp599). The twelve transmembrane (TM1 to TM12) alpha helices are labelled with the black dotted box. The red shadow periods refer to the identical residues, the yellow shadow periods refer to the conservative substitutions. (B) Sequence alignment of the regions of TM1, 3, 6, 8 and 10. Residues that primarily contribute to the S1 binding site of hSERT, hNET and hDAT were labelled with green dotted box.

3.4. Potential application to the pharmacology of human monoamine transporters

As for human monoamine transmitters (MATs), there are three homologous transporters (hSERT, hNET and hDAT) being responsible for the reuptake of the biogenic amine neurotransmitters (serotonin, norepinephrine and dopamine) from the synapse into the presynaptic nerve terminal [41,42]. Deficiency of certain neurotransmitters is responsible for a variety of mood disorders such as major depression [40], schizophrenia and Parkinson's disease [43,44], and development of drugs inhibiting hSERT, hNET and hDAT is thus an important strategy for treatment of such diseases [45,46]. Therefore, there is an urgently need to explore the binding of various drugs to the corresponding MATs targets.

The reported X-ray structure of hSERT [9] has provided insight into the serotonin transporter pharmacology. However, the structures of another two MATs hNET and hDAT still remain elusive. It is important to note that hSERT/hNET/hDAT share greater than 50% sequence identity between each other, as shown in Figure 10(A). Particularly, Figure 10(B) indicates a sequence alignment of the TM1, 3, 6, 8 and 10 regions that primarily contribute to the central binding site of the transporter showed that 62% (hSERT and hNET), 57% (hSERT and hDAT) and 85% (hNET and hDAT) are conserved. Even though the crystal structure of a given hNET or hDAT is not available, the reliable working model to study

the pharmacology of hSERT based on the crystal structure of dDAT by combining computational homology modelling, molecular docking, MD simulation and binding free energy calculation provides a remarkable choice to facilitate drug discovery procedure targeting MATs.

4. Conclusion

The solving of hSERT X-ray crystallographic structure is a significant event along the history of antidepressant drug design, and the crystal structure of hSERT provided the chance to reassess the homology model constructed based on *drosophila melanogaster* dopamine transporter (dDAT) in previous publication. The comparison in this work proved the homology model is geometrically close to the reported X-ray crystallographic structure. And side-chain conformations of the 11 residues composing ligand-binding pocket matched well with that in the crystal structure. In addition, MD simulations for the escitalopram-hSERT complex revealed consistent structural features for drug binding as reported previously. Moreover, it is believed that the procedure by applying integrated computational methods is feasible to study the pharmacology of human MATs such as hNET and hDAT using dDAT or hSERT crystal structure as a template.

Disclosure statement

There is no conflict of interest in this manuscript.

Funding

This work was funded by the Program for New Century Excellent Talents in University (NCET-13-0632); National Natural Science Foundation of China [21505009]; Precision Medicine Project of the National Key Research and Development Plan of China [2016YFC0902200]; Innovation Project on Industrial Generic Key Technologies of Chongqing [cstc2015zdcy-ztxz120003].

References

- [1] Zheng G, Xue W, Wang P, et al. Exploring the inhibitory mechanism of approved selective norepinephrine reuptake inhibitors and reboxetine enantiomers by molecular dynamics study. *Sci Rep.* **2016**;6:26883.
- [2] Kaplan C, Zhang Y. Assessing the comparative-effectiveness of antidepressants commonly prescribed for depression in the US Medicare population. *J Ment Health Policy Econ.* **2012**;15:171–178.
- [3] Lopez-Munoz F, Alamo C. Monoaminergic neurotransmission: the history of the discovery of antidepressants from 1950s until today. *Curr Pharm Des.* **2009**;15:1563–1586.
- [4] Li YH, Wang PP, Li XX, et al. The human kinome targeted by FDA approved multi-target drugs and combination products: a comparative study from the drug-target interaction network perspective. *PLOS ONE.* **2016**;11:1–15.
- [5] Xu J, Wang P, Yang H, et al. Comparison of FDA approved kinase targets to clinical trial ones: insights from their system profiles and drug-target interaction networks. *BioMed Res Int.* **2016**;2016:2509385.
- [6] Marazziti D, Landi P, Baroni S, et al. The role of platelet/lymphocyte serotonin transporter in depression and beyond. *Curr Drug Targets.* **2013**;14:522–530.
- [7] Petersen CI, DeFelice LJ. Ionic interactions in the *Drosophila* serotonin transporter identify it as a serotonin channel. *Nat Neurosci.* **1999**;2:605–610.
- [8] Zhu F, Shi Z, Qin C, et al. Therapeutic target database update 2012: a resource for facilitating target-oriented drug discovery. *Nucleic Acids Res.* **2012**;40:D1128–D1136.
- [9] Coleman JA, Green EM, Gouaux E. X-ray structures and mechanism of the human serotonin transporter. *Nature.* **2016**;532:334–339.
- [10] Andersen J, Olsen L, Hansen KB, et al. Mutational mapping and modeling of the binding site for (S)-citalopram in the human serotonin transporter. *J Biol Chem.* **2010**;285:2051–2063.
- [11] Andersen J, Stuhr-Hansen N, Zachariassen LG, et al. Molecular basis for selective serotonin reuptake inhibition by the antidepressant agent fluoxetine (prozac). *Mol Pharmacol.* **2014**;85:703–714.
- [12] Andersen J, Taboureau O, Hansen KB, et al. Location of the antidepressant binding site in the serotonin transporter: importance of ser-438 in recognition of citalopram and tricyclic antidepressants. *J Biol Chem.* **2009**;284:10276–10284.
- [13] Yan A, Wang L, Xu S, et al. Aurora-A kinase inhibitor scaffolds and binding modes. *Drug Discovery Today.* **2011**;16:260–269.
- [14] Rao HB, Zhu F, Yang GB, et al. Update of PROFEAT: a web server for computing structural and physicochemical features of proteins and peptides from amino acid sequence. *Nucleic Acids Res.* **2011**;39:W385–W390.
- [15] Penmatsa A, Wang KH, Gouaux E. X-ray structure of dopamine transporter elucidates antidepressant mechanism. *Nature.* **2013**;503:85–90.
- [16] Xue W, Wang P, Li B, et al. Identification of the inhibitory mechanism of FDA approved selective serotonin reuptake inhibitors: an insight from molecular dynamics simulation study. *Phys Chem Chem Phys.* **2016**;18:3260–3271.
- [17] Arnold K, Bordoli L, Kopp J, et al. The SWISS-MODEL workspace: a web-based environment for protein structure homology modelling. *Bioinformatics.* **2006**;22:195–201.
- [18] Laskowski RA, MacArthur MW, Moss DS, et al. PROCHECK: a program to check the stereochemical quality of protein structures. *J Appl Cryst.* **1993**;26:283–291.
- [19] Wang H, Goehring A, Wang KH, et al. Structural basis for action by diverse antidepressants on biogenic amine transporters. *Nature.* **2013**;503:141–145.
- [20] The PyMOL Molecular Graphics System, Version 1.8 Schrödinger, LLC.
- [21] Sobolev V, Eyal E, Gerzon S, et al. SPACE: a suite of tools for protein structure prediction and analysis based on complementarity and environment. *Nucleic Acids Res.* **2005**;33:W39–W43.
- [22] Wiederstein M, Sippl MJ. ProSA-web: interactive web service for the recognition of errors in three-dimensional structures of proteins. *Nucleic Acids Res.* **2007**;35:W407–W410.
- [23] Sippl MJ. Recognition of errors in three-dimensional structures of proteins. *Proteins.* **1993**;17:355–362.
- [24] Humphrey W, Dalke A, Schulten K. VMD: visual molecular dynamics. *J Mol Graphics.* **1996**;14:33–38, 27–28.
- [25] Sorensen L, Andersen J, Thomsen M, et al. Interaction of antidepressants with the serotonin and norepinephrine transporters: mutational studies of the S1 substrate binding pocket. *J Biol Chem.* **2012**;287:43694–43707.
- [26] Kaminski GA, Fries RA, Tirado-Rives J, et al. Evaluation and reparametrization of the OPLS-AA force field for proteins via comparison with accurate quantum chemical calculations on peptides. *J Phys Chem B.* **2001**;105:6474–6487.
- [27] Lomize MA, Pogozheva ID, Joo H, et al. OPM database and PPM web server: resources for positioning of proteins in membranes. *Nucleic Acids Res.* **2012**;40:D370–D376.
- [28] Wu EL, Cheng X, Jo S, et al. CHARMM-GUI Membrane Builder toward realistic biological membrane simulations. *J Comput Chem.* **2014**;35:1997–2004.
- [29] Hornak V, Abel R, Okur A, et al. Comparison of multiple Amber force fields and development of improved protein backbone parameters. *Proteins.* **2006**;65:712–725.
- [30] Dickson CJ, Madej BD, Skjevik AA, et al. Lipid14: the amber lipid force field. *J Chem Theory Comput.* **2014**;10:865–879.
- [31] Glide v. 5.5. Schrödinger, LLC. New York (NY); **2009**.
- [32] Hara Y, Murayama S. Effects of analgesic-antipyretics on the spinal reflex potentials in cats: An analysis of the excitatory action of aminopyrine. *Nihon yakurigaku zasshi Folia pharmacologica Japonica.* **1992**;100:383–390.
- [33] Springborg M, Kirtman B. Efficient vector potential method for calculating electronic and nuclear response of infinite periodic systems to finite electric fields. *J Chem Phys.* **2007**;126:104107.
- [34] Kollman PA, Massova I, Reyes C, et al. Calculating structures and free energies of complex molecules: combining molecular mechanics and continuum models. *Acc Chem Res.* **2000**;33:889–897.
- [35] Xu L, Sun H, Li Y, et al. Assessing the performance of MM/PBSA and MM/GBSA methods. 3. The impact of force fields and ligand charge models. *J Phys Chem B.* **2013**;117:8408–8421.
- [36] Sun H, Li Y, Tian S, et al. Assessing the performance of MM/PBSA and MM/GBSA methods. 4. Accuracies of MM/PBSA and MM/GBSA methodologies evaluated by various simulation protocols using PDBbind data set. *Phys Chem Chem Phys: PCCP.* **2014**;16:16719–16729.
- [37] Sun H, Li Y, Shen M, et al. Assessing the performance of MM/PBSA and MM/GBSA methods. 5. Improved docking performance using high solute dielectric constant MM/GBSA and MM/PBSA rescoring. *Phys Chem Chem Phys: PCCP.* **2014**;16:22035–22045.
- [38] Chen F, Liu H, Sun H, et al. Assessing the performance of the MM/PBSA and MM/GBSA methods. 6. Capability to predict protein-protein binding free energies and re-rank binding poses generated by protein-protein docking. *Phys Chem Chem Phys: PCCP.* **2016**;18:22129–22139.
- [39] Froesner GG, Peterson DA, Deinhardt FW, et al. Transmission of hepatitis A and hepatitis B by shared needle. *Lancet.* **1973**;301:1183.
- [40] Wang P, Yang F, Yang H, et al. Identification of dual active agents targeting 5-HT1A and SERT by combinatorial virtual screening methods. *Bio-Med Mater Eng.* **2015**;26(s1):S2233–S2239.
- [41] Kristensen AS, Andersen J, Jorgensen TN, et al. SLC6 neurotransmitter transporters: structure, function, and regulation. *Pharmacol Rev.* **2011**;63:585–640.
- [42] Zhu F, Han B, Kumar P, et al. Update of TTD: therapeutic target database. *Nucleic Acids Res.* **2010**;38:D787–D791.

- [43] Iversen L. Neurotransmitter transporters: fruitful targets for CNS drug discovery. *Mol Psychiatry*. 2000;5:357–362.
- [44] Li YH, Xu JY, Tao L, et al. SVM-prot 2016: a web-server for machine learning prediction of protein functional families from sequence irrespective of similarity. *PLOS ONE*. 2016;11:e0155290.
- [45] Immadisetty K, Madura JD. A review of monoamine transporter-ligand interactions. *Curr Comput Aided Drug Des*. 2013;9:556–568.
- [46] Yang H, Qin C, Li YH, et al. Therapeutic target database update 2016: enriched resource for bench to clinical drug target and targeted pathway information. *Nucleic Acids Res*. 2016;44:D1069–D1074.